



MicroRNA profiling in cutaneous wounds of diabetic rats

Y.-F. Liu^{1,2}, M. Ding², D.-W. Liu¹, Y. Liu¹, Y.-G. Mao¹ and Y. Peng¹

¹First Affiliated Hospital of Nanchang University, Nanchang, China

²Guangzhou Integrated Traditional Chinese and Western Medicine Hospital, Guangzhou, China

Corresponding author: D.-W. Liu

E-mail: dewuliu@126.com

Genet. Mol. Res. 14 (3): 9614-9625 (2015)

Received January 7, 2015

Accepted May 25, 2015

Published August 14, 2015

DOI <http://dx.doi.org/10.4238/2015.August.14.24>

ABSTRACT. Despite years of effort, current therapies for diabetic wounds are still not fully efficacious. Emerging evidence has suggested that microRNAs (miRNAs) play key roles in multiple physiological and pathological processes in eukaryotes, and could potentially be powerful therapeutic tools. This study investigated the differential expression profiling of miRNAs in cutaneous wounds in streptozotocin-induced diabetic rats and normal rats, and its significance in diabetic wound healing. Using microarrays, 18 miRNAs were identified as being upregulated and 65 as being downregulated in the diabetic group. The miRNA profiling results were validated by quantitative reverse transcriptase polymerase chain reaction. Finally, functional annotation analysis using the DAVID and miR2Subpath databases revealed that the differentially expressed miRNAs were involved in MAPK signaling pathways, the Wnt signaling pathway, and other signaling pathways that may be closely linked to wound healing. This study provides an experimental foundation for further investigation of mechanisms that underlie poor diabetic wound healing, and of miRNA-based therapies that are associated with wound healing.

Key words: Diabetes mellitus, experimental; Skin; Wound healing; MicroRNA profiling

INTRODUCTION

Diabetes mellitus is increasingly prevalent. Previous studies have established that the ability to heal wounds is severely impaired in diabetic patients (Morain and Colen, 1990), and poor wound healing can result in morbidity or death. Although significant progress has been made, the current therapeutic approaches are still not effective (Cavanagh et al., 2005), and the economic burden of the treatment is great. Hence, there is a need for a better understanding of the mechanisms that underlie this diabetic complication, in order to develop therapies that are more effective.

MicroRNAs (miRNAs) are short non-coding RNAs and can efficiently induce posttranscriptional gene repression, which renders them a potentially powerful therapeutic tool. It is estimated that they can target over 1000 human miRNAs and about 60% of human protein-coding genes (Bartel, 2009), and are involved in almost all of the signal transduction pathways. Recent evidence has indicated that miRNAs play key roles in multiple physiological and pathological processes in eukaryotes, such as stage development, organ development, cell differentiation, signal transduction, metabolism, and tumorigenesis. Consequently, numerous investigators have attempted to ascertain their relevance in disease in order to develop miRNA-based therapies, which restore the molecular and cellular processes required for successful healing. Several miRNAs are specifically expressed in the skin and its appendages (Yi et al., 2006; Aberdam et al., 2008), and some of them are closely related to wound healing (Banerjee and Sen, 2013). However, few studies have been conducted on diabetic wound healing.

In this study, we explored the differential expression profiling of miRNAs in cutaneous wounds in streptozotocin (STZ)-induced diabetic rats and normal rats using miRNA microarray assays, and investigated the mechanism that underlies poor diabetic wound healing in order to provide a theoretical and experimental foundation for future studies.

MATERIAL AND METHODS

Diabetic rat model and sample harvest

All of the animal studies were conducted in accordance with a protocol approved by the Institutional Review Board of Nanchang University. Young male Sprague-Dawley rats (weighing 180-200 g) were obtained from the Laboratory Animal Center of Nanchang University, and housed in an environmentally controlled facility on a 12-h light/dark cycle. A week later, six rats (weighing 230-250 g) were randomly selected for induction of the STZ-induced type 1 diabetic model, by intraperitoneal injection of a single dose of STZ (Sigma-Aldrich, St. Louis, MO, USA) at 65 mg/kg body weight in 50 mM citrate buffer, pH 4.0 (Group A). Six control animals received an equal volume of citrate buffer (Group B). Blood glucose levels were measured on 3, 7, 14, 21, and 28 days after injection, and food and water intake, as well as the animals' health, were monitored throughout the study. Animals with blood glucose levels exceeding 300 mg/dL were deemed diabetic and were used in the study. Four weeks after the onset of diabetes, the animals were anesthetized and the dorsal hair was clipped and depilated. Dorsal skin was marked with a standardized template (3.14 cm²) and excised to create a full-thickness dorsal excisional wound. After surgery, wounds were covered with normal dressings that were changed daily, using only physiological saline to clean the wounds. All of the rats were housed separately and provided with free access to water and standard rodent chow. On day 3, the

wound tissue was harvested and dissected, and then equal amounts of it from the same group were pooled, immediately immersed in liquid nitrogen, and stored at -80°C until use.

RNA isolation and microarray experiment

The total RNAs were extracted from the samples using TRIzol reagent (Invitrogen, Grand Island, NY, USA) according to the manufacturer protocol, and quantified by spectrophotometry (NanoDrop ND-1000, Wilmington, DE, USA). RNA quality was assessed by formaldehyde-denaturing gel electrophoresis. Total RNA was purified using the mirVana™ miRNA isolation kit (Ambion, Austin, TX, USA) and quantified again. A total of 200 ng purified RNA was labeled with fluorescein Cy3, and hybridization was conducted using an Agilent Rat miRNA 8X15K microarray (Agilent Technologies, Santa Clara, CA, USA), which provides full coverage of all known rat miRNAs (677 unique mature miRNAs, based on miRBase V. 16.0, <http://www.mirbase.org>), according to manufacturer protocol. After the microarray slides were washed, hybridization signals were detected by scanning the slides. Data were extracted using Agilent Feature Extraction Software V. 10.7, normalized using the Agilent GeneSpring GX 10.0 software, and differences between the groups were analyzed. miRNAs were considered to be differentially expressed if they exhibited more than a two-fold expression difference between the two groups.

Quantitative reverse transcriptase polymerase chain reaction (qRT-PCR) for miRNA expression analysis

To validate the miRNA microarray data, rno-miR-150 and rno-miR-31 were selected for qRT-PCR assays using fluorescent nucleic acid dye (SYBR® Green I) on a 7900HT Fast Real-Time PCR System (Applied Biosystems), and snRNA U6 was selected as the normalization control. All of the primers (miRNA RT primer and PCR primers) were synthesized by Invitrogen (Table 1). Briefly, 100 ng of the purified total RNA was reverse transcribed under the following conditions: 16°C for 10 min, 37°C for 30 min, and 65°C for 5 min. The conditions for the PCR were as follows: 95°C for 10 min, followed by 40 cycles at 95°C for 15 s and 60°C for 1 min. All of the reactions were run in triplicate. A melting curve analysis was performed at $60^{\circ}\text{--}95^{\circ}\text{C}$, temperature ramp 2%. Subsequently, 2–4 μL miRNA of the real time PCR products were used to confirm the specificity of the RT-PCR by 1.5% nondenaturing-agarose gel electrophoresis. The relative expression level of each miRNA, which was represented as a crossing threshold (Ct), was calculated using the following equation: $2^{-\Delta\text{Ct}}$, where $\Delta\text{Ct} = \text{Ct}_{\text{miRNA}} - \text{Ct}_{\text{U6}}$. The fold change of each miRNA was calculated using the equation $2^{-\Delta\Delta\text{Ct}}$.

Table 1. Sequences of the genes and primers used for the real-time reverse transcriptase polymerase chain reaction.

Gene or primer	Sequence 5'→3'
U6-Forward	CTCGCTTCGGCAGCACA
U6-Reverse	AACGCTTCACGAATTTGCGT
miRNA universal sense primer	GTGCAGGGTCCGAGGT
rno-miR-150	TCTCCCAACCTTGTACCACTG
rno-miR-150-RT	GTCGTATCCAGTGCAGGGTCCGAGGTATTCCGACTGGATACGACcactgg
rno-miR-150-AS	GAGTCTCCCAACCCCTGTACCA
rno-miR-31	AGGCAAGATGCTGGCATAGCTG
rno-miR-31-RT	GTCGTATCCAGTGCAGGGTCCGAGGTATTCCGACTGGATACGACcagcta
rno-miR-31-AS	ACTAGGCAAGATGCTGGCATAG

Functional annotation and pathway analysis

To understand the functions of the differentially expressed miRNAs, we identified the target genes of the miRNAs by integrating three public databases (TargetScan, miRDB, and miRanda). The target genes were then annotated by KEGG pathway enrichment analysis using the DAVID database (<http://david.abcc.ncifcrf.gov/home.jsp>) (Huang et al., 2009a,b). In addition, we performed pathway enrichment analysis using the miR2Subpath database (<http://202.97.205.78:8080/miR2Subpath/index.jsp>), which considers a miRNA as a regulator of a signaling pathway if the miRNA target genes are significantly enriched in the signaling pathway ($P < 0.001$). We then identified several signaling pathways that are implicated in wound healing and some of the differentially expressed miRNAs that are involved in these signaling pathways. Finally, we performed a PubMed (<http://www.ncbi.nlm.nih.gov/pubmed/>) literature search using “miRNA” as a key word, in order to retrieve all relevant publications and compile a list of known functions of the miRNAs.

RESULTS

Diabetic rat phenotype

The experimental rats became hyperglycemic three days after STZ injection, and remained hyperglycemic (blood glucose levels exceeding 426.6 mg/dL at each time point) before being killed for tissue harvesting. Water intake was approximately 280 mL/day, food intake was about 56 g/day, and body weight averaged 290 g on the day of surgery. The same parameters for the control group were approximately 50 mL/day, 45 g/day, and 410 g/rat, respectively. The experimental rats were significantly thinner and smaller than the control rats, and had matted and withered coats (Figure 1).

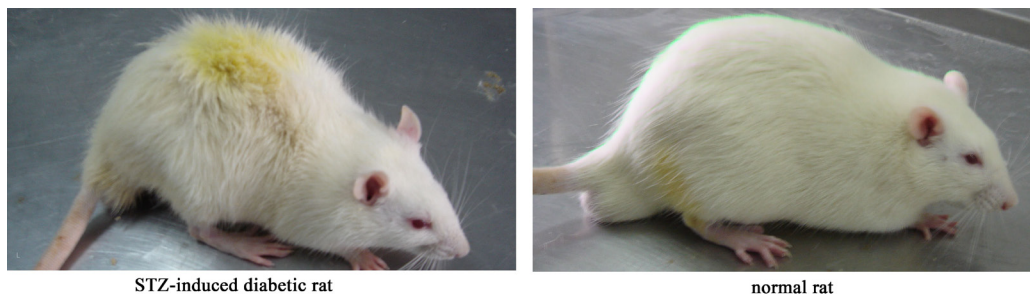


Figure 1. Phenotypes of streptozotocin-induced diabetic and control rats.

Total RNA quality

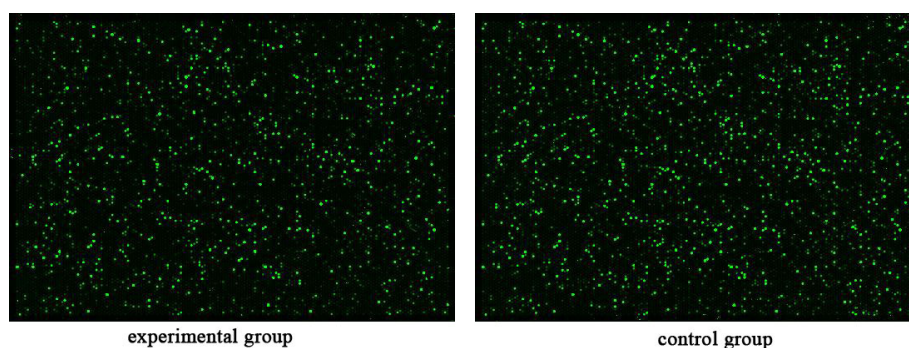
The purities, concentrations, and weights of the total RNAs all met the experimental requirements (Table 2). An electropherogram of the formaldehyde-denaturing gel electrophoresis indicated that the electrophoretic strips were clear and that the strip brightness of 28S:18S rRNA approached 2:1, suggesting good integrity.

Table 2. Quality of the total RNA in cutaneous wound tissue isolated from streptozotocin-induced diabetic rats and control rats.

Group	Total amount (µg)	A260/280	A260/230	Concentration (µg/µL)
A	95.6	1.93	1.73	1.249
B	54.0	1.91	1.22	0.716

miRNA expression profiling in cutaneous wounds of STZ-induced diabetic and control rats

Scanned images of the hybridized miRNA microarray of the STZ-induced diabetic and control rats are shown in Figure 2. Eighty-three miRNAs were identified, 18 of which were upregulated (Table 3) and 65 were downregulated (Table 4) in diabetic cutaneous wounds. A scatter plot of the fluorescence ratio was generated to visualize the differentially expressed miRNAs (Figure 3).

**Figure 2.** Scanned images of the hybridized microarray of miRNAs in cutaneous wounds of streptozotocin-induced diabetic and control rats.**Table 3.** Upregulated miRNAs detected in cutaneous wounds of streptozotocin-induced diabetic rats.

miRNA	miRBase accession No.*	Total probe signal (A)	Total probe signal (B)	Fold change (A vs B)
rno-miR-496-5p	MIMAT0017372	71.0868	0.1	1049.6483
rno-miR-105	MIMAT0012825	43.6151	0.1	644.0087
rno-miR-466c-5p	MIMAT0005279	31.6145	0.1	466.8112
rno-miR-122-5p	MIMAT0000827	29.675	0.1	438.1729
rno-miR-331-5p	MIMAT0017033	21.4106	0.1	316.1431
rno-miR-338-5p	MIMAT0004646	8.90167	0.1	131.4397
rno-miR-674-5p	MIMAT0005329	8.78381	0.1	129.6994
rno-miR-539-5p	MIMAT0003176	104.0009	31.98064	4.8018
rno-miR-297	MIMAT0000899	55.8271	20.18888	4.0831
rno-miR-466d	MIMAT0017824	503.926	205.12729	3.6274
rno-miR-465-5p	MIMAT0012850	252.347	132.6893	2.8081
rno-miR-672-5p	MIMAT0005327	739.271	414.651	2.6325
rno-miR-3593-5p	MIMAT0017896	24.6128	14.6116	2.4872
rno-miR-32-3p	MIMAT0017103	785.362	470.40698	2.4652
rno-miR-466b-5p	MIMAT0005278	1279.352	803.567	2.3508
rno-miR-382-5p	MIMAT0003201	54.708	36.148	2.2347
rno-miR-150-5p	MIMAT0000853	349.40732	232.0625	2.2232
rno-miR-30c-1-3p	MIMAT0004719	46.7544	33.947838	2.0336

*<http://www.mirbase.org/>.

Table 4. Downregulated miRNAs detected in cutaneous wounds of streptozotocin-induced diabetic rats.

miRNA	miRBase accession No.*	Total probe signal (A)	Total probe signal (B)	Fold change (B vs A)
rno-miR-196a-5p	MIMAT0000871	0.1	84.9508	575.3241
rno-miR-134-5p	MIMAT0000840	0.1	52.8724	358.0749
rno-miR-425-3p	MIMAT0017306	0.1	48.446198	328.0988
rno-miR-484	MIMAT0005319	0.1	47.28	320.2008
rno-miR-31-3p	MIMAT0017102	0.1	46.9324	317.8467
rno-miR-328a-3p	MIMAT0000564	0.1	44.155098	299.0376
rno-miR-96-5p	MIMAT0000818	0.1	43.4803	294.4677
rno-miR-338-3p	MIMAT0000581	0.1	43.024002	291.3773
rno-miR-218a-5p	MIMAT0000888	0.1	42.9384	290.7977
rno-miR-3564	MIMAT0017837	0.1	41.9004	283.7678
rno-miR-878	MIMAT0005286	0.1	41.6103	281.8032
rno-miR-204-5p	MIMAT0000877	0.1	37.277	252.4561
rno-miR-466b-1-3p	MIMAT0017285	0.1	36.74054	248.8230
rno-miR-378a-5p	MIMAT0003378	0.1	35.0034	237.0583
rno-miR-455-5p	MIMAT0005316	0.1	34.5202	233.7859
rno-miR-30a-3p	MIMAT0000809	0.1	33.589897	227.4854
rno-miR-743a-3p	MIMAT0005334	0.1	32.1871	217.9851
rno-miR-222-3p	MIMAT0000891	0.1	31.817799	215.4840
rno-miR-542-3p	MIMAT0003179	0.1	31.7279	214.8752
rno-miR-532-3p	MIMAT0005323	0.1	31.4367	212.9031
rno-miR-335	MIMAT0000575	0.1	29.2803	198.2990
rno-miR-346	MIMAT0000596	0.1	28.90421	195.7519
rno-miR-341	MIMAT0000587	0.1	28.5619	193.4337
rno-miR-1188-5p	MIMAT0017854	0.1	27.9521	189.3038
rno-miR-3557-3p	MIMAT0017820	0.1	27.7546	187.9663
rno-miR-322-3p	MIMAT0000547	0.1	23.0238	155.9272
rno-miR-144-3p	MIMAT0000850	0.1	21.9334	148.5426
rno-miR-423-5p	MIMAT0017305	0.1	21.7068	147.0079
rno-miR-678	MIMAT0012857	0.1	21.45811	145.3237
rno-miR-331-3p	MIMAT0000570	0.1	20.6477	139.8352
rno-miR-542-5p	MIMAT0003178	0.1	20.0021	135.4630
rno-miR-127-3p	MIMAT0000833	0.1	19.827	134.2771
rno-miR-363-3p	MIMAT0003210	0.1	19.1364	129.6001
rno-miR-449a-5p	MIMAT0001543	0.1	18.7991	127.3157
rno-miR-200c-3p	MIMAT0000873	0.1	18.1336	122.8087
rno-miR-30e-3p	MIMAT0004720	0.1	17.7143	119.9690
rno-miR-362-5p	MIMAT0012828	0.1	17.488	118.4364
rno-miR-186-5p	MIMAT0000863	0.1	17.4838	118.4079
rno-miR-379-5p	MIMAT0003192	0.1	16.0689	108.8256
rno-miR-34b-5p	MIMAT0000813	0.1	15.8732	107.5002
rno-miR-434-3p	MIMAT0005315	0.1	14.9947	101.5507
rno-miR-291a-3p	MIMAT0000895	0.1	14.8156	100.3377
rno-miR-182	MIMAT0005300	0.1	14.4833	98.0872
rno-miR-154-5p	MIMAT0000856	0.1	14.0399	95.0843
rno-miR-34c-5p	MIMAT0000814	0.1	13.8955	94.1064
rno-miR-877	MIMAT0005285	0.1	13.60205	92.1190
rno-miR-192-5p	MIMAT0000867	0.1	13.4023	90.7662
rno-miR-493-3p	MIMAT0003191	0.1	13.3178	90.1940
rno-miR-667-3p	MIMAT0012852	0.1	12.64	85.6036
rno-miR-181a-1-3p	MIMAT0000884	0.1	12.2416	82.9055
rno-miR-3561-5p	MIMAT0017830	0.1	11.9473	80.9123
rno-miR-328b-3p	MIMAT0017904	0.1	11.9015	80.6022
rno-miR-674-3p	MIMAT0005330	0.1	9.0774	61.4761
rno-miR-339-3p	MIMAT0004648	0.1	8.38338	56.7759
rno-miR-351-5p	MIMAT0000608	0.1	7.55103	51.1389
rno-miR-191-3p	MIMAT0017146	0.1	6.99531	47.3753
rno-miR-23a-5p	MIMAT0004712	0.1	6.68763	45.2916
rno-let-7d-3p	MIMAT0000563	0.1	6.10358	41.3361
rno-miR-31-5p	MIMAT0000810	27.0221	206.66501	5.1796
rno-miR-770-3p	MIMAT0017317	18.7092	117.31551	4.2466
rno-miR-125a-3p	MIMAT0004729	10.038	51.37843	3.4664
rno-miR-503-5p	MIMAT0003213	32.4069	154.1989	3.2225
rno-miR-196b-5p	MIMAT0001082	21.3282	88.2556	2.8024
rno-miR-450a-5p	MIMAT0001547	18.0602	55.8997	2.0962
rno-miR-874-3p	MIMAT0005284	10.7577	32.6481	2.0553

*<http://www.mirbase.org/>.

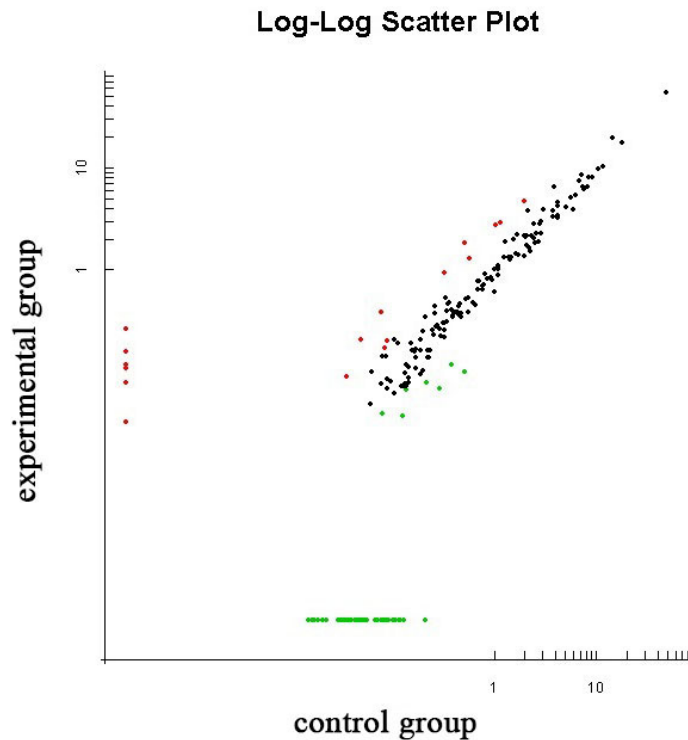


Figure 3. Scatter plot for fluorescence signal intensity of the miRNAs in two samples. Both axes represent the fluorescence signal intensity of the miRNAs in chips, and each point represents the fluorescence signal intensity of one probe set (miRNA). Red points indicate an A:B ratio ≥ 2 (upregulated genes), green points indicate an A:B ratio ≤ 0.5 (downregulated genes), and black points indicate A:B ratios that were between 0.5 and 2.

Verification of the microarray data by qRT-PCR

To verify our array results, we performed qRT-PCR assays on selected miRNAs (rno-miR-150 and rno-miR-31) from the STZ-induced diabetic rats and controls (three times each). Amplification and dissociation curve charts for rno-miR-150, rno-miR-31, and snRNA U6 were generated (Figure 4), and 1.5% nondenaturing-agarose electrophoresis was performed to evaluate the RT-PCR. The qRT-PCR data revealed that rno-miR-150 increased by up to 2.63-fold more in diabetic wound tissue than in normal wound tissue, whereas rno-miR-31 decreased by 3.64-fold. These results are similar to the differential expression detected by the array analysis, and demonstrate that miRNAs were significantly upregulated or downregulated in the diabetic wound tissue in comparison with the normal wound tissue ($P < 0.005$; Figure 5). The dissociation curve chart shows that all of the curves were unimodal, indicating the specificity of the amplified product. The 1.5% nondenaturing-agarose gel electrophoresis revealed that all of the electrophoretic bands of the RT-PCR products were clear, and the length of all of the RT-PCR products was approximately 100 bp. All of these data suggest that the results of the RT-PCR were accurate.

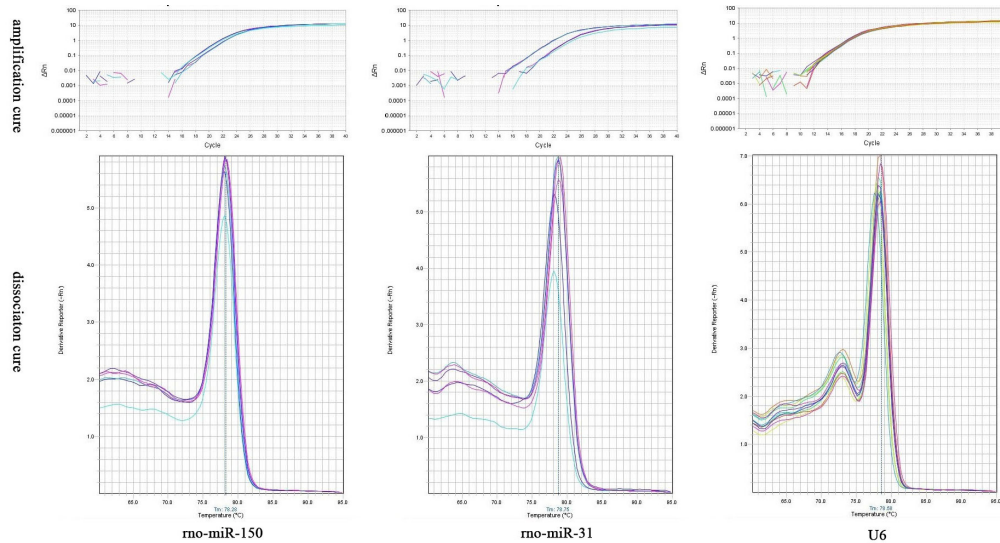


Figure 4. Amplification and dissociation curve charts for rno-miR-150, rno-miR-31, and snRNA U6. In the amplification curve chart, the x-axis represents cycle number and the y-axis represents the real-time fluorescence signal intensity of the corresponding cycle number. In the dissociation curve chart, the x-axis represents the temperature of the reverse transcriptase polymerase chain reaction (RT-PCR) products and the y-axis represents the real-time fluorescence-signal-intensity change rate with increasing temperature. Differently colored curves correspond to different RT-PCRs.

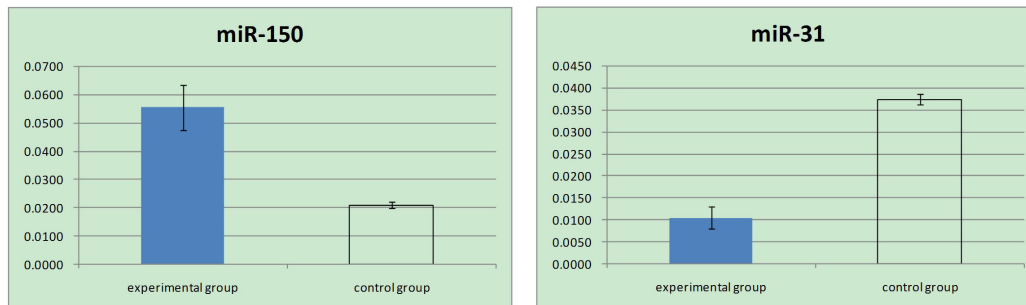


Figure 5. Relative expression levels of miR-150 (A) and miR-31 (B) in cutaneous wound tissue isolated from streptozotocin-induced diabetic rats (filled bars, N = 3) and control rats (open bars, N = 3) by quantitative reverse transcriptase polymerase chain reaction, normalized to snRNA U6, and calculated using the following equation: $2^{-\Delta Ct}$, where $\Delta Ct = Ct_{miRNA} - Ct_{U6}$. Values are reported as means \pm SDs.

Functional annotation and pathway analysis

In all, 835 target genes of the differentially expressed miRNAs were obtained, according to the criterion that targets predicted by all three public databases were considered putative candidates. The results of the enrichment analysis revealed that 20 KEGG pathways were significantly enriched ($P < 0.05$), and the MAPK signaling pathway was the most enriched

(Table 5). Pathway enrichment analysis using the miR2Subpath database revealed that several signaling pathways that are associated with wound healing were enriched, and some of the differentially expressed miRNAs were involved in these pathways (Table 6).

Table 5. Predicted functions of differentially expressed miRNA target genes.

KEGG pathway	Count	%	P value
MAPK signaling pathway	31	4.6	7.00E-06
Adipocytokine signaling pathway	12	1.8	2.70E-04
Oocyte meiosis	15	2.2	7.10E-04
Long-term potentiation	11	1.6	1.10E-03
Colorectal cancer	11	1.6	4.70E-03
Pancreatic cancer	10	1.5	5.00E-03
Amyotrophic lateral sclerosis	9	1.3	6.40E-03
Neurotrophin signaling pathway	14	2.1	6.60E-03
Long-term depression	9	1.3	1.30E-02
Chemokine signaling pathway	16	2.4	1.60E-02
Cell cycle	13	1.9	1.60E-02
TGF-beta signaling pathway	10	1.5	2.00E-02
Cytokine-cytokine receptor interaction	17	2.5	2.50E-02
Prostate cancer	10	1.5	2.60E-02
T cell receptor signaling pathway	11	1.6	3.40E-02
GnRH signaling pathway	10	1.5	3.40E-02
p53 signaling pathway	8	1.2	3.60E-02
ECM-receptor interaction	9	1.3	3.80E-02
Wnt signaling pathway	13	1.9	4.30E-02
Apoptosis	9	1.3	4.80E-02

Table 6. KEGG pathways implicated in wound healing and involving differentially expressed miRNAs.

KEGG pathway	Wound healing-related functions*	miRNAs involved
MAPK signaling pathway	Involved in various cellular functions, including cell proliferation, differentiation, and migration	miR-31, -204, -335, -127, -34b/c, -182, -150, let-7d
Wnt signaling pathway	Involved in cell-fate specification, progenitor-cell proliferation, cell division, cell adhesion, and motility	miR-222, -542, -346, -200c, -186, -182, -150,
VEGF signaling pathway	Mediate the proliferation and migration of endothelial cells and promote their survival and vascular permeability	miR-222
Notch signaling pathway	Involved in cell proliferation, differentiation, apoptosis, and mediate intercellular interactions	miR-449a, -34c
TGF-beta signaling pathway	Regulate cellular functions such as proliferation, apoptosis, differentiation, and migration	miR-186, -154, -192
ErbB signaling pathway	Regulate cellular functions such as proliferation, differentiation, motility, and survival	miR-222, -200c, -34b/c, -150
Insulin signaling pathway	Associated with the MAPK pathway and mitogenic responses, and involved in glycogen synthesis and glucose uptake of cell	miR-338, -150, -346, -542, -34b
T cell receptor signaling pathway	Associated with cytokine production and the immune system	miR-222, -150
Axon guidance	Precisely regulate axons to reach their correct targets, and important in neural development	miR-134, -204, -222, -346, -200c, -34b, -181a, -339, -23a, -31
Focal adhesion	Involved in cell motility, proliferation, differentiation, survival, and regulation of gene expression	miR-539, -134, -96, -455, -222, -542, -200c, -34b/c, -23a, -150, -338
Regulation of actin cytoskeleton	Maintain cell architecture, and involved in cell motility, differentiation, and intra-cellular transportation	miR-96, -222, -363, -200c, -182, -34c, -23a, -122, -338
ECM-receptor interaction	Involved in cell adhesion, migration, differentiation, proliferation, and apoptosis	miR-196a, -96, -338, let-7d
Adherens junction	Maintain tissue architecture and cell polarity, and limit cell movement and proliferation	miR-455, 449, 186, 34c, 328
Cell adhesion molecules	Involved in hemostasis, immune response, inflammation, and development of neuronal tissue	miR-496

*Based on the KEGG pathway database (<http://www.kegg.jp/kegg/pathway.html#organismal>).

DISCUSSION

The present study compared the miRNA profiling of cutaneous wound tissue between STZ-induced diabetic rats and normal rats by microarray, and validated the microarray data by qRT-PCR assays. Eighty-three miRNAs were identified in STZ-induced diabetic wound samples, with 18 miRNAs upregulated and 65 downregulated. A previous study found that the expression of some specific miRNAs changed at a specific phase of wound healing, and the aberrant regulation of these specific miRNAs plays a key role in the abnormal healing of problem wounds (Shilo et al., 2007). Recent advances in the synthesis and chemistry of nucleic acids have allowed us to establish more efficient methods of performing miRNA-based therapies *in vitro* and *in vivo*, and multiple approaches of miRNA modulation have been used in clinical and experimental applications, with great success (Lanford et al., 2010; HatziaPOSTOLOU et al., 2011; Zhu et al., 2011; Creasey et al., 2014). Therefore, miRNA targeting alone, or in combination with conventional therapies, could be a new opportunity for diabetic wound healing, by reducing aberrantly expressed miRNA levels or by elevating beneficial miRNA levels. In addition, miRNA-based therapies provide a unique advantage, because by modulating a single miRNA a group of functionally related genes in a pathway can be targeted, in contrast to modulating a single gene at a time, as is the case with conventional gene therapy. In this regard, our study may provide a theoretical and experimental foundation for the further investigation of miRNA-based therapies, which may reveal a novel mechanism of impaired diabetic wound healing at the molecular level.

The enrichment analysis of the differentially expressed miRNAs showed that several miRNAs are involved in several KEGG pathways that can regulate the proliferation, differentiation, apoptosis, migration, and secretion of tissue repair cells, and are linked to inflammatory cells, the extracellular matrix, growth factors, and other relevant factors (Table 6). It has been reported that wound healing is tightly regulated by multiple factors, and any abnormal changes to these factors may impair optimum wound healing (Baum and Arpey, 2005). We suggest that differentially expressed miRNAs probably contribute to poor diabetic wound healing, and this requires further investigation.

We found that miR-331 was upregulated in the cutaneous wounds of STZ-induced diabetic rats, whereas miR-425 was downregulated. miR-331 has been reported to target the mRNA of the enzyme deoxyhypusine hydroxylase, which can catalyze the activation of the eukaryotic translation initiation factor and thus inhibit cell proliferation (Epis et al., 2012). miR-425 has been reported to negatively regulate the atrial natriuretic peptide (Arora et al., 2013), which can inhibit multiple cell proliferation, indicating that expression alteration of both miRNAs may impair diabetic wound healing because they inhibit cell proliferation. miR-484 suppresses the translation of the mitochondrial fission protein Fis1, and consequently inhibits Fis1-mediated fission and apoptosis in cardiomyocytes and adrenocortical cancer cells (Wang et al., 2012). miR-378 enhances cell survival and promotes angiogenesis by targeting *Sufu* and *Fus1* expression (Lee et al., 2007), and miR-30 inhibits mitochondrial fission and the consequent apoptosis by suppressing p53 expression (Li et al., 2010), and stimulates arteriolar branching by directly targeting the Notch ligand Delta-like 4 (*Dll4*) (Jiang et al., 2013). All of these miRNAs were downregulated in the cutaneous wounds of STZ-induced diabetic rats in our study, suggesting that alterations may contribute to impaired wound healing by increasing cell apoptosis and inhibiting angiogenesis. In addition, we found that miR-200 was downregu-

lated in the experimental group, which was reported to be highly expressed in normal skin and was expected to positive regulate E-cadherin by specifically targeting *ZEB1* and *SIP1* (also known as *ZEB2*) (Gregory et al., 2008; Korpál et al., 2008) and thus was seemed to be essential in maintaining epithelial stability (Tunggal et al., 2005), suggesting that it has an inhibitory effect on diabetic wound healing.

In conclusion, this study has identified differentially expressed miRNAs in cutaneous wound tissue of STZ-induced diabetic rats using microarray analysis, and provides evidence that they are involved in the process of wound healing, which suggests that the alteration of these miRNAs may be a novel molecular mechanism of impaired diabetic wound healing. Together with the great progress that has been made in miRNA-based therapies, this study may provide a new method for the treatment of poor diabetic wound healing, once the relevant theories have been sufficiently elucidated. Nevertheless, our study only serves as a start toward a deeper understanding of the roles of miRNAs in diabetic wound healing. Their exact regulatory functions are still unclear, and how to perform miRNA-based therapy effectively and safely still needs further study.

Conflicts of interest

The authors declare no conflicts of interest.

ACKNOWLEDGMENTS

Research supported by the National Natural Science Foundation of China (#30560058 and #81060323).

REFERENCES

- Aberdam D, Candi E, Knight RA and Melino G (2008). miRNAs, 'stemness' and skin. *Trends Biochem. Sci.* 33: 583-591.
- Arora P, Wu C, Khan AM, Bloch DB, et al. (2013). Atrial natriuretic peptide is negatively regulated by microRNA-425. *J. Clin. Invest.* 123: 3378-3382.
- Banerjee J and Sen CK (2013). MicroRNAs in skin and wound healing. *Methods Mol. Biol.* 936: 343-356.
- Bartel DP (2009). MicroRNAs: target recognition and regulatory functions. *Cell* 136: 215-233.
- Baum CL and Arpey CJ (2005). Normal cutaneous wound healing: clinical correlation with cellular and molecular events. *Dermatol. Surg.* 31: 674-686.
- Cavanagh PR, Lipsky BA, Bradbury AW and Botek G (2005). Treatment for diabetic foot ulcers. *Lancet* 366: 1725-1735.
- Creasey KM, Zhai J, Borges F, Van Ex F, et al. (2014). miRNAs trigger widespread epigenetically activated siRNAs from transposons in *Arabidopsis*. *Nature* 508: 411-415.
- Epis MR, Giles KM, Kalinowski FC, Barker A, et al. (2012). Regulation of expression of deoxyhypusine hydroxylase (DOHH), the enzyme that catalyzes the activation of eIF5A, by miR-331-3p and miR-642-5p in prostate cancer cells. *J. Biol. Chem.* 287: 35251-35259.
- Gregory PA, Bert AG, Paterson EL, Barry SC, et al. (2008). The miR-200 family and miR-205 regulate epithelial to mesenchymal transition by targeting ZEB1 and SIP1. *Nat. Cell Biol.* 10: 593-601.
- Hatziaepostolou M, Polytarchou C, Aggelidou E, Drakaki A, et al. (2011). An HNF4 α -miRNA inflammatory feedback circuit regulates hepatocellular oncogenesis. *Cell* 147: 1233-1247.
- Huang DW, Sherman BT and Lempicki RA (2009a). Systematic and integrative analysis of large gene lists using DAVID bioinformatics resources. *Nat. Protoc.* 4: 44-57.
- Huang DW, Sherman BT and Lempicki RA (2009b). Bioinformatics enrichment tools: paths toward the comprehensive functional analysis of large gene lists. *Nucleic Acids Res.* 37:1-13.
- Jiang Q, Lagos-Quintana M, Liu D, Shi Y, et al. (2013). miR-30a regulates endothelial tip cell formation and arteriolar branching. *Hypertension* 62: 592-598.

- Korpál M, Lee ES, Hu G and Kang Y (2008). The miR-200 family inhibits epithelial-mesenchymal transition and cancer cell migration by direct targeting of E-cadherin transcriptional repressors ZEB1 and ZEB2. *J. Biol. Chem.* 283: 14910-14914.
- Lanford RE, Hildebrandt-Eriksen ES, Petri A, Persson R, et al. (2010). Therapeutic silencing of microRNA-122 in primates with chronic hepatitis C virus infection. *Science* 327: 198-201.
- Lee DY, Deng Z, Wang CH and Yang BB (2007). MicroRNA-378 promotes cell survival, tumor growth, and angiogenesis by targeting SuFu and Fus-1 expression. *Proc. Natl. Acad. Sci. U. S. A.* 104: 20350-20355.
- Li J, Donath S, Li Y, Qin D, et al. (2010). miR-30 regulates mitochondrial fission through targeting p53 and the dynamin-related protein-1 pathway. *PLoS Genet.* 6: e1000795.
- Morain WD and Colen LB (1990). Wound healing in diabetes mellitus. *Clin. Plast. Surg.* 17: 493-501.
- Shilo S, Roy S, Khanna S and Sen CK (2007). MicroRNA in cutaneous wound healing: a new paradigm. *DNA Cell Biol.* 26: 227-237.
- Tunggal JA, Helfrich I, Schmitz A, Schwarz H, et al. (2005). E-cadherin is essential for *in vivo* epidermal barrier function by regulating tight junctions. *EMBO J.* 24: 1146-1156.
- Wang K, Long B, Jiao JQ, Wang JX, et al. (2012). miR-484 regulates mitochondrial network through targeting Fis1. *Nat. Commun.* 3: 781.
- Yi R, O'Carroll D, Pasolli HA, Zhang Z, et al. (2006). Morphogenesis in skin is governed by discrete sets of differentially expressed microRNAs. *Nat. Genet.* 38: 356-362.
- Zhu H, Hu F, Wang R, Zhou X, et al. (2011). *Arabidopsis* Argonaute10 specifically sequesters miR166/165 to regulate shoot apical meristem development. *Cell* 145: 242-256.